



# Effects of different loading methods in molecular dynamics on deformation behavior of polymer crystals

Koki Yoshida<sup>1</sup> · Kensuke Kageyama<sup>1</sup> · Takenobu Sakai<sup>1</sup>

Received: 14 July 2023 / Accepted: 21 September 2023  
© The Author(s), under exclusive licence to Springer Nature B.V. 2023

## Abstract

Thermoplastics have a crystal structure. It has been pointed out that the crystalline structure affects viscoelastic behavior in crystalline polymers, which must be taken into account in MD simulations. In this study the crystalline lamellar structure of Polyethylene (PE) was reproduced via molecular dynamics. To investigate the mechanical behavior and deformation behavior of the lamellar structure of PE, deformation was applied to the model under a constant tensile rate and constant tensile load as tensile and creep analyses, respectively. A tensile analysis indicated localized cracking, and a creep analysis revealed molecular-chain undulation along the tensile direction. To clarify the reason for the difference in deformation distribution between tensile and creep analyses, the potential energy during tensile loading was examined. In the tensile analysis, all the potential energies increased at the start of tension development and decreased rapidly at the break. As revealed in the creep analysis, the bond stretching and bond angle potential energies did not change when deformation started at a strain of approximately 0.20. These results indicated that the deformation behavior depended on the loading configuration, such as tensile and creep loading, and that deformation behaviors vary because of differences in displacement distribution and potential energy.

**Keywords** Polyethylene · Lamellar structure · Molecular dynamic simulation · Constant-load analysis · Constant-strain rate analysis

## 1 Introduction

Thermoplastic resins are widely used in mechanical parts and building components because of their excellent workability and lightweight, and most thermoplastic resins have the crystalline and amorphous structure as crystalline polymers. Their crystalline structures and crystallinity have been studied experimentally and analytically.

Parenteau et al. (2012) investigated the relationship between the crystalline structure and mechanical properties of polypropylene (PP) with different crystallinities and crystal thicknesses. Ayoub et al. (2011) investigated the effects of crystallinity on the mechanical properties of PP, both experimentally and using a micromechanical model, and found that PP

---

✉ T. Sakai  
sakai@mech.saitama-u.ac.jp

<sup>1</sup> Graduate School of Science and Engineering, Saitama University, Tokyo, Japan

responds like an elastomer at low crystallinity and exhibits a thermoplastic-like response as the crystallinity increases. Um et al. (2021) evaluated the mechanical properties of carbon fiber and polyethylene terephthalate composites with different crystallinities and found that the composites with higher crystallinity exhibited better properties, including improved storage moduli, high-temperature stability, and shear properties. Other studies have also indicated that the crystallinity of composites affects their mechanical properties (Dusunceli and Colak 2008; Felder et al. 2020; Ahzi et al. 2003; Galeski 2003; Kong and Hay 2002), including our studies (Sakai et al. 2021; Fukushima et al. 2021; Somiya et al. 2006).

Several studies on crystalline polymers using molecular dynamics (MD) simulations have been performed. Hossain et al. (2010) applied uniaxial tensile deformation to an amorphous polyethylene (PE) model via MD to investigate the effects of the chain length, number of chains, strain rate, and temperature on the stress–strain behavior. Vu-Bac et al. (2014) performed a uniaxial tensile analysis on an amorphous PE model via MD and found that the temperature, followed by the strain rate, had the highest influence on the yield stress and modulus. Koyanagi et al. (2020) also performed a uniaxial tensile analysis on an amorphous PA6 model and presented a quantitative method for predicting the experimental value of the tensile strength of a polymer material by using molecular dynamics. In other studies, crystalline polymers were analyzed using models created for amorphous structures for understanding the void creation (Mahajan et al. 2010), deformation (Higuchi 2019; Shang et al. 2015), free volume evaluation (Bowman et al. 2019), time-temperature superposition principle (Khare and Phelan 2020; Liu et al. 2009), and chain mobility (Capaldi et al. 2002). However, as mentioned previously, the crystallinity affects the mechanical properties of crystalline polymers. Therefore it is necessary to adopt a model that includes the crystal structure in the MD simulations.

Yeh et al. (2020) showed that in MD simulations, PE crystal models consisting of finite-length molecular chains exhibit deformation closer to that of the actual material under tensile deformation than models consisting of infinite-length molecular chains. O'Connor and Robbins (2016) reproduced PE crystals with finite lengths via MD and performed a tensile analysis in the crystal axis direction. They found that the yield stress increased in proportion to the molecular-chain length and was saturated at an experimental value of 6.6 GPa. In-Chul et al. (2017, 2015) created a semicrystalline PE model consisting of crystalline and amorphous layers and found positive correlations between the crystal thickness and the elastic modulus and yield stress. Additionally, they found that a model with the crystal axis parallel to the tensile direction had a smaller yield strain than a model with the crystal axis tilted in the tensile direction. Moyassari et al. (2018, 2019) created a PE crystal structure with a bimodal molar mass distribution via MD by cooling it from the molten state and subjecting it to tensile deformation; they found that the elastic modulus and yield stress were higher for models with shorter molecular chains. Ikeshima et al. (2019) added water molecules to a semicrystalline model of polyamide 6 (PA6) created via MD and found that the penetration of water molecules into the boundary between the crystalline phase and the amorphous layer reduced the PA6 elastic modulus and yield strength. As described above, tensile deformation has been applied to a model that combines amorphous and crystalline structures. However, in these studies, deformation in the crystal axis direction or oblique to it was applied, since the crystal axis is perpendicular to the lamellar crystal axis inside a lamellar crystal oriented in the direction of the tensile axis of a spherulite crystal (Nitta 1999) and the orientation of the crystal obtained when cooling from the melted state is random (Moyassari et al. 2019). In the experimental study, Nitta and Nomura (2014) suggested that the occurrence of deformation failure of the lamellar clusters in the equator direction of the spherulites and the yield mechanism observed on the stress-strain curve strongly suggest that the failure of the lamellar clusters in the equator direction is the cause. Here the lamellar clusters in the equator

direction are oriented perpendicular to the loading direction. To clarify the cause of this, it is necessary to understand the deformation behavior of the lamellar structure perpendicular to the crystal axis direction.

Since polymers are viscoelastic, they exhibit viscoelastic behavior. It is known that the presence of crystals also affects this viscoelastic behavior. Pan et al. (2016) conducted creep tests under various temperatures and loads on oscillatory shear injection molding and conventional injection molding specimens and found that the former exhibited better creep properties than the latter because of their higher crystallinity. Tábi et al. (2016) reported that poly(lactic acid) with a higher content of highly ordered  $\alpha$ -crystals exhibits better creep properties. Other experimental studies have also indicated that the crystal structure affects the viscoelastic behavior in crystalline polymers (Sakai and Somiya 2011; Boey et al. 1995; Sakai et al. 2018), and it is necessary to consider the viscoelastic behavior in MD simulations and to understand the effect of crystalline structure on viscoelastic behavior by MD, especially lamellar structure; however, there are not any researches about the deformation of lamellar structure.

In this study, the lamellar structure of PE was reproduced via MD simulations, and tensile deformation was applied perpendicular to the crystal axis direction under a constant strain rate and constant applied load, as tensile and creep analyses, respectively. The main objective was to clarify the mechanical, viscoelastic, and fracture behaviors of lamellar structures of PE.

## 2 Methodology

### 2.1 Analysis conditions

Gromacs 2020.04 was used as the analysis software (Berendsen et al. 1995), OPLS-AA, which is a commonly used force field of all atomic models, was used, and the boundary conditions were periodic for stability of analysis (Jorgensen et al. 1996). The Nose–Hoover (Nosé 1984; Hoover 1985) and Parrinello–Rahman (Rahman and Parrinello 1980) methods were employed for temperature and pressure control, respectively. The time increment was set to 1 fs. The following potential energies were used in the analysis: (1) bond stretching potential energy  $U_{bond}$ , (2) bond angle potential energy  $U_{angle}$ , (3) torsion angle potential energy  $U_{dihedral}$ , and (4) nonbonding potential energy  $U_{nonbonding}$ . Here  $U_{nonbonding}$  is the sum of the Lennard–Jones (LJ) and Coulomb potential energies, which are defined as follows (Jorgensen et al. 1996):

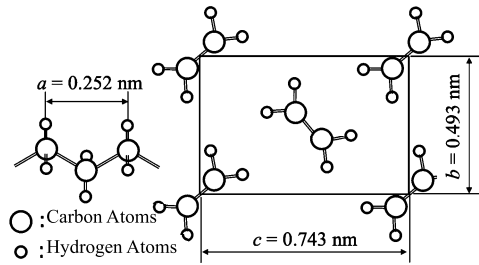
$$U_{bond}(r) = \frac{1}{2}k_r(l - l_0)^2, \quad (1)$$

$$U_{angle}(\theta) = \frac{1}{2}k_\theta(\theta - \theta_0)^2, \quad (2)$$

$$U_{dihedral}(\varphi) = k \sum_i \frac{V_1^i}{2} [1 + \cos(\varphi_i + f_{i1})] + \frac{V_2^i}{2} [1 - \cos(2\varphi_i + f_{i2})] + \frac{V_3^i}{2} [1 + \cos(3\varphi_i + f_{i3})], \quad (3)$$

$$U_{nonbonding}(r) = U_{LJ}(r) + U_C(r) = 4\varepsilon \left\{ \left( \frac{\sigma}{r} \right)^{12} - \left( \frac{\sigma}{r} \right)^6 \right\} + f \frac{q_i q_j}{\varepsilon_r r_{ij}}. \quad (4)$$

Fig. 1 PE lattice parameters



Here  $U$  is the energy,  $k$  is the force coefficient,  $V$  is the Fourier coefficient,  $l_0$ ,  $\theta_0$ ,  $\phi_0$  are the reference values,  $\sigma$  and  $\epsilon$  are the Lennard–Jones radial and depth,  $q$  is the atomic charge, and  $r$  is the interatomic distance.

## 2.2 Lamellar structure model creation

To make a lamellar structure of PE, 160 molecular chains with a polymerization degree of 30 (total molecular weight: 134,720) were arranged in a cell according to the lattice constant of the PE crystal (Kohji 1993) (Fig. 1). Then the model was used to simulate the minimized and equilibrated energy in an isothermal–isovolumetric variation (constant number of particles  $N$ ; volume  $V$ ; temperature  $T$ , as in  $NVT$ ) ensemble at 300 K for 20 ps. At the first time, relaxation analyses were done for several nanoseconds; however, the relaxation was completed in the first 10 ps. Therefore 20 ps was adopted as the relaxation time—which is twice as much as the obtained value.

Five models were created via the above procedure. In the following section, the results for one of these models are presented.

## 2.3 Tensile analysis

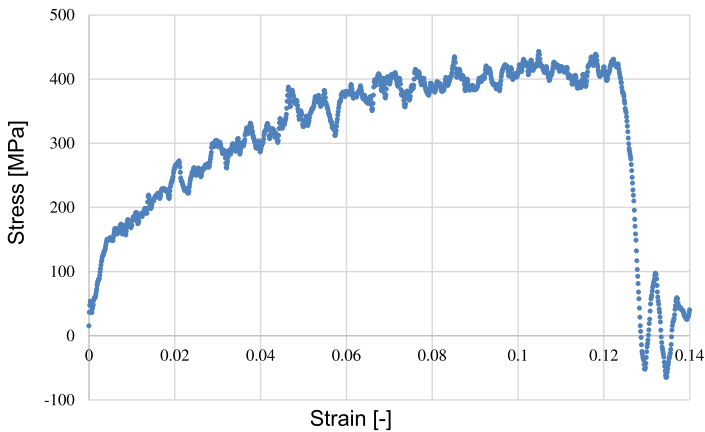
Tensile analysis was performed at a constant strain rate, and creep analysis was performed at a constant applied load. For tensile analysis, the model was deformed in the tensile direction at a strain rate of  $10^9 \text{ s}^{-1}$  at 300 K in the  $NVT$  ensemble. The  $NVT$  ensemble ignores volume changes such as thermal expansion; however, it considers volume changes due to deformation. In this study, the evaluation was performed by varying the velocity from  $10^{-7} \text{ s}^{-1}$ , which is the strain rate at which normal computer analysis is realistically possible, to  $10^{-11} \text{ s}^{-1}$ , which is close to the velocity of the initial displacement in creep in this study. However, since almost similar results were obtained at all strain rates, the result of  $10^{-9} \text{ s}^{-1}$  was adopted for evaluation in this paper.

For creep analysis, the model was subjected to tensile loads of 40, 200, and 400 MPa at 300 K in the isothermal–isobaric variation  $NPT$  ensemble. In both analyses, the tensile direction was perpendicular to the molecular chain.

# 3 Results and discussion

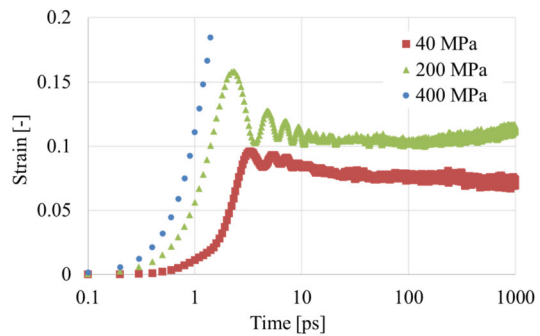
## 3.1 Tensile analysis under constant strain rate

Figure 2 shows the stress–strain curve for the tensile analysis. During the initial deformation stage, the stress increased rapidly. The elastic modulus was 6.3 GPa. The rate of stress increase decreased as the deformation progressed. As the strain increased, the stress increased



**Fig. 2** Stress–strain curve for the tensile analysis (Color figure online)

**Fig. 3** Strain–time curves for the creep analysis with different applied load (Color figure online)



at a decreasing rate, reaching a maximum value of 421 MPa. After the strain reached 0.125, the stress rapidly decreased.

### 3.2 Tensile analysis under constant applied load

The strain–time curves for the creep analyses with the different applied loads are shown in Fig. 3. First, the creep analysis was performed with applied load of 40 MPa, which was approximately 10% of the tensile strength revealed in the tensile analysis. From the start of loading to 3 ps, the strain increased to approximately 0.1. Thereafter, the strain decreased, indicating the absence of creep deformation. Next, a constant load of 200 MPa, which was approximately 50% of the tensile strength, was applied. The strain increased from 0, reaching approximately 0.16 at 2.5 ps, and then remained constant, indicating the absence of creep. Therefore, to examine the creep behavior, the analysis was performed with applied stress of 400 MPa, which is equivalent to the tensile strength. In this case the strain increased. The results indicate that a large amount of stress is required for creep deformation of the crystal. We discuss the creep analysis results obtained with applied load of 400 MPa.

### 3.3 Appearance of deformation for different loading configurations

A comparison of the model used in the tensile and creep analysis was performed. Snapshots of the model used in the tensile analysis are shown in Fig. 4. No significant visible changes

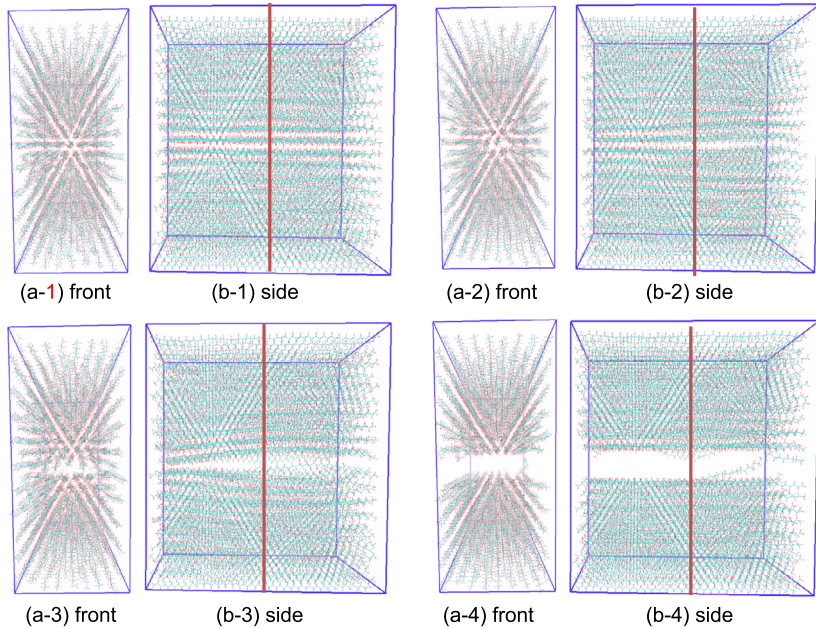


**Fig. 4** (a) Front and (b) side molecular structures in the tensile analysis (strain: (1) 0.122, (2) 0.124, (3) 0.126, (4) 0.129) (Color figure online)

were observed in the stress–strain curve up to a strain of 0.122—immediately before a large reduction in stress. When the strain reached 0.124, i.e., the strain at which the stress began to decrease, undulation was observed in the molecular chains near the right of center in each deformation diagram of side view, and some cracks became wider than others. As the strain increased to 0.126, during the stress reduction, the undulation region expanded, and the cracks widened. When the strain reached 0.129, the stress decreased to approximately zero, the undulation of the molecular chain almost disappeared, and the molecular chains returned to a linear form. As the strain increased, the cracks widened. Similar analyses were performed for the other models, yielding different failure points. Therefore the failure points were attributed to inhomogeneities in the models.

Figure 5 shows snapshots of the model used in the creep analysis. No visible changes were observed in the model until the strain reached 0.10. When the strain reached 0.28, slight molecular-chain undulation was observed throughout the model. The degree of undulation was larger at a strain of 0.41, and it increased with the strain. When the strain reached 0.60, voids were observed between the molecular chains, as if they were being peeled from each other.

In the tensile analysis, a large displacement was observed only in the molecular chains around the fracture area, whereas in the creep analysis, molecular-chain displacement was observed throughout the model. It is considered that the strain rate affects the deformation state. The constant strain rate test was performed at  $10^9/s$ , whereas the strain rate in the constant load test was approximately  $10^{11}/s$ . Although details are omitted here, the state of deformation in the constant strain rate test at  $10^{11}/s$  was identical to that at  $10^9/s$ , confirming that the strain rate had no effect.



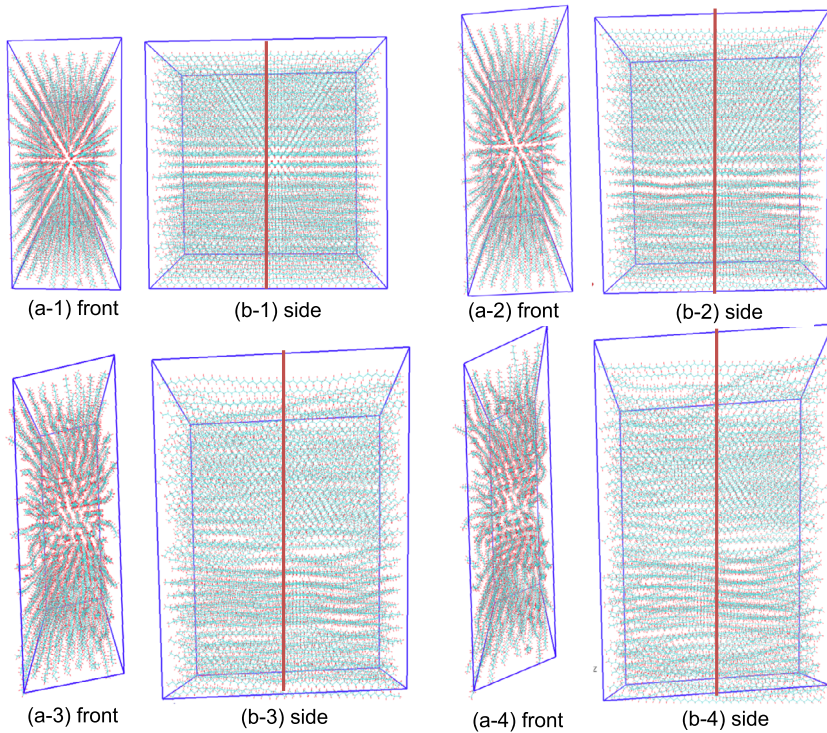


**Fig. 5** (a) Front and (b) side molecular structures in the creep analysis (400 MPa) (strain: (1) 0.10, (2) 0.28, (3) 0.41, (4) 0.60) (Color figure online)

### 3.4 Displacement distribution in tensile analysis

The aforementioned difference in molecular-chain displacement may be due to differences in the distribution of atoms moving to the major fracture point. The displacement distribution, which is the number of atoms moving as tension started to develop at the cross section marked by the red line in Figs. 4 and 5, is shown in Fig. 6. For the tensile analysis (Fig. 6(a)), at a strain of 0.122, the snapshot did not show any large fracture points; however, the displacement distribution indicated large displacement near the fracture points. When the strain reached 0.124, the snapshot showed undulation in the molecular chain, and the displacement distribution indicated that the displacement around the undulation was large. When the strain increased to 0.126, the degree of undulation increased, and the range of large displacements widened. At a strain of 0.129, the large-displacement distribution was even wider. The different models used in the analysis tended to exhibit large amounts of tension near the fracture point. From this we assume that the heterogeneity of the model may trigger displacement, which may be the cause of fracture.

For the creep analysis (Fig. 6(b)), at a strain of 0.10, the snapshot did not show any major fracture points, but the displacement distribution indicated that the atoms moved over a wide area on the right side of the model. When the strain reached 0.28, the molecular chains began to undulate, as shown in the snapshots, and the displacement distribution increased. As the strain increased to 0.41 and 0.60, the degree of molecular-chain undulation increased as the displacement distribution broadened.

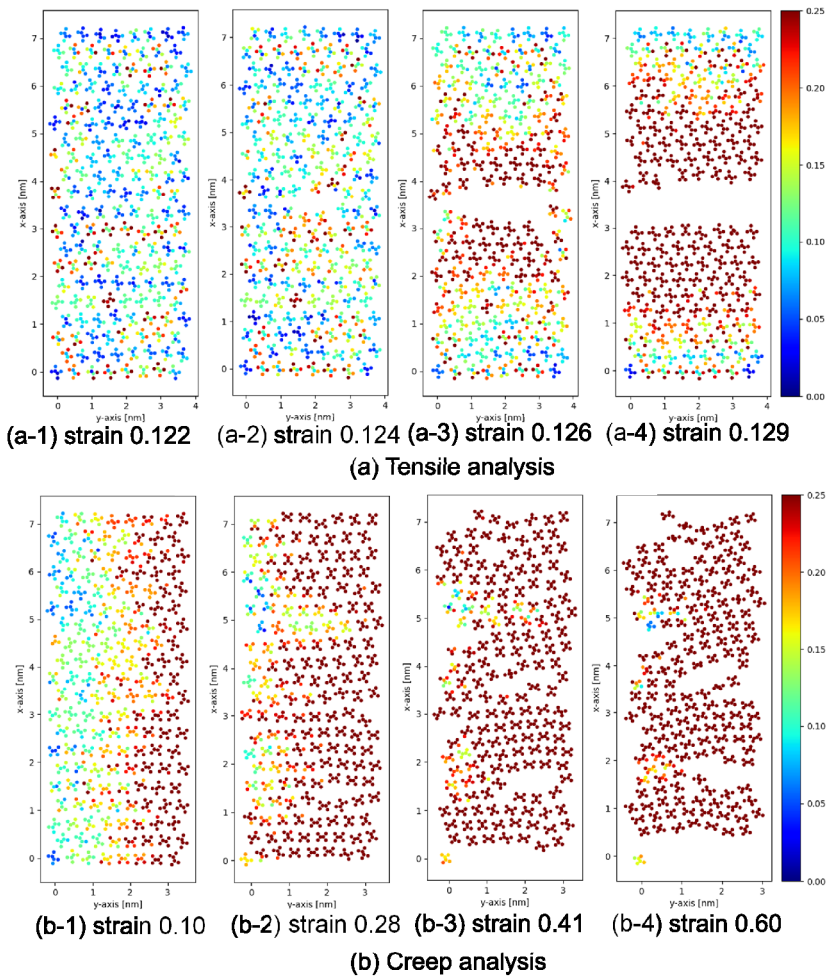


**Fig. 6** Displacement distributions revealed in (a) tensile analysis and (b) creep analysis (Color figure online)

In the tensile analysis, the material is forced to deform at a constant rate; therefore the internal structure was deformed without relaxation, and the deformation was concentrated in structurally unstable areas. In contrast, in the creep analysis, deformation was not forced; thus deformation occurred along with relaxation. Therefore the entire model was deformed. This difference may be due to the difference in failure modes due to the different loading methods.

### 3.5 Potential energy in tensile analysis

To consider the reason for the displacement distribution differences, the potential energies of the two loading configurations were compared. The potential energy in the tensile analysis is shown in Fig. 7. The bond stretching potential energy (Fig. 7(a)) gradually increased as the strain increased to approximately 0.126. With a further increase in the strain to 0.137, it decreased sharply. Similarly, the bond angle potential energy (Fig. 7(b)) increased up to a



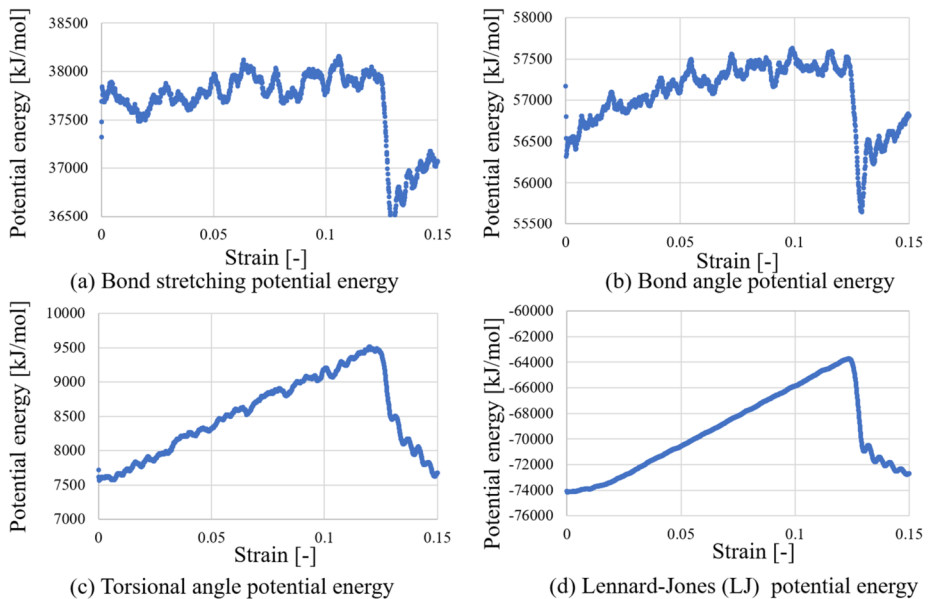


**Fig. 7** Potential energy in the tensile analysis (Color figure online)

strain of approximately 0.126 and decreased sharply with a further increase in the strain to 0.137. Therefore the bond angle potential energy increased in a same manner from the bond stretching potential energy. As revealed in the tensile analysis, the torsion angle (Fig. 7(c)) and LJ (Fig. 7(d)) potential energies increased nearly linearly to a strain of approximately 0.126 and decreased sharply from that point to a strain of 0.137. As described above, for both types of potential energies, an increase was observed as tension started to develop. A rapid decrease was observed when the strain reached 0.126, and the potential energy almost returned to its initial level. According to these results and the displacement distribution (Fig. 6(a)), the atoms that exhibited a large displacement within a narrow range in the displacement distribution moved to unstable positions, reached the potential energy limit, and the lamellar structure broke.

The potential energy in the creep analysis is shown in Fig. 8. The bond stretching potential energy (Fig. 8(a)) gradually decreased as the strain increased to approximately 0.20. Subsequently, as the strain increased to approximately 0.30, the bond stretching potential energy increased slightly and then began to decrease. The bond angle potential energy (Fig. 8(b)) remained constant up to a strain of approximately 0.20. From there it increased as the strain increased to 0.30, and it then began to decrease, similarly to the bond stretching potential energy. The torsion angle potential energy (Fig. 8(c)) increased rapidly from the start of loading to a strain of 0.20; thereafter, it increased slowly and then increased rapidly again as the strain increased to 0.30. The LJ potential energy (Fig. 8(d)) increased slightly from the start of tensile loading to a strain of approximately 0.20, and the rate of increase increased as the strain increased from 0.20 to approximately 0.30. The snapshots and potential energies were compared, and no significant deformation was observed in the molecular chain until the strain reached 0.20, when the first change was observed for all potential energies. However, beyond a strain of 0.20, when a change in potential energy occurred, molecular-chain undulation started to be observed in the snapshot. In the snapshots

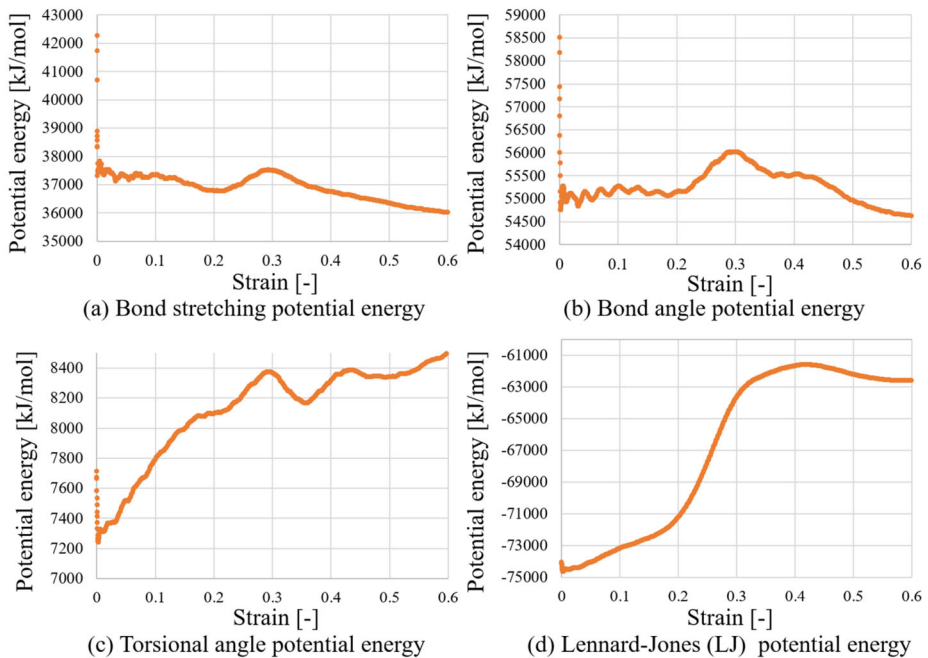


**Fig. 8** Potential energy in the tensile analysis (Color figure online)

taken after the strain reached 0.30, when the second change in potential energy occurred, voids were observed between the molecular chains, indicating a relationship between the molecular-chain deformation and potential-energy change. Up to a strain of 0.20, the bond stretching and bond angle potential energies remained almost unchanged, whereas the torsion angle and LJ potential energies increased. The displacement distribution in Fig. 6(b) indicated that large displacements in the tensile direction occurred throughout the model from one side in the vertical direction. This deformation suggesting that the torsion angle and nonbonding distance moved over a wide range of unstable positions with tensile deformation. When the strain exceeded 0.20, in addition to the torsion angle and the nonbonding distance, the bonding distance and bond angle became unstable, indicating extensive fracture with molecular-chain undulation. As indicated above, the tensile analysis revealed that the bonding distance, angle, and nonbonding distance become unstable in the movable parts of the model owing to the forced displacement, reaching their limits and causing large deformation.

In contrast, as indicated by the creep analysis, the deformation progressed as the bonding distance and bond angle moved to stable positions throughout the model; after the strain exceeded 0.20, they began to move to unstable positions over a wide range, resulting in large deformations. These factors are considered to be responsible for the localized cracking in the tensile analysis and the overall unraveling deformation in the creep analysis.

This differs from the results of Higuchi (2019) when pulled parallel to the crystal axis. In this case, crystals and amorphous are stacked. The molecules constituting the crystal bonded to the amorphous are then pulled along with the deformation, causing the amorphous part to crystallize and the crystal to break down. This is considered to be the same as the creep analysis in this study, as the amorphous part acts as a buffer, and a relaxation phenomenon occurs in the crystal. Moreover, the crystallinity of the models in Higuchi's study increased

with the stretching the models in parallel and perpendicular directions; however, the lamellar structure of our model loosened and failed, and the crystallinity decreased. Determining the crystallinity of the model was difficult because it was necessary to consider not only the degree of orientation, but also the waviness due to the loosening of the lamellar structure. We will discuss the relationship between crystallinity and the deformation in the future.

In this study, it is clear that cracks form when the pull-out of molecules constituting the crystal is inhibited by the absence of amorphous parts, but under conditions where relaxation phenomena occur, the crystal structure loosens and collapses in the same way as in Higuchi's and Nitta's results.

## 4 Conclusion

The pure crystalline structure of PE was reproduced via MD, and tensile and creep analyses were carried out. The deformation behavior observed in the tensile analysis showed localized cracking, whereas in the creep analysis, molecular-chain undulation in the tensile direction was observed throughout the model. Regarding the displacement distribution during deformation, the tensile analysis revealed large displacements around the fracture area, whereas the creep analysis revealed large displacements in the load direction throughout the model. The potential energy during deformation increased rapidly from the start of loading in the tensile analysis and increased gradually in the creep analysis. It is clear that cracks form when the pull-out of molecules constituting the crystal is inhibited by the absence of amorphous parts, but under conditions where relaxation phenomena occur, the crystal structure loosens and collapses.

**Acknowledgements** This work was supported by JSPS KAKENHI (Grant Numbers JP19KK0363 and JP21H01221).

**Author contributions** Yoshida analyze every data, Sakai and Kageyama supervised Yoshida, and Yoshida and Sakai wrote the main manuscript text and prepared every figures. All authors reviewed the manuscript.

## Declarations

**Ethical approval** The work described in the paper has not been published before. It is not under consideration for publication elsewhere, and the publication has been approved by all coauthors.

**Competing interests** The authors declare no competing interests.

## References

- Ahzi, S., Makradi, A., Gregory, R.V., et al.: Modeling of deformation behavior and strain-induced crystallization in poly(ethylene terephthalate) above the glass transition temperature. *Mech. Mater.* **35**(12), 1139–1148 (2003)
- Ayoub, G., Zaïri, F., Fréderix, C., et al.: Effects of crystal content on the mechanical behaviour of polyethylene under finite strains: experiments and constitutive modelling. *Int. J. Plast.* **27**(4), 492–511 (2011)
- Berendsen, H.J.C. van der Spoel, D., van Drunen, R.: GROMACS: a message-passing parallel molecular dynamics implementation. *Commun. Comput. Phys.* **91**(1–3), 43–56 (1995)
- Boey, F.Y.C., Lee, T.H., Khor, K.A.: Polymer crystallinity and its effect on the non-linear bending creep rate for a polyphenylene sulphide thermoplastic composite. *Polym. Test.* **14**(5), 425–438 (1995)
- Bowman, A.L., Mun, S., Nouranian, S., et al.: Free volume and internal structural evolution during creep in model amorphous polyethylene by molecular dynamics simulations. *Polymer* **170**, 85–100 (2019)

- Capaldi, F.M., Boyce, M.C., Rutledge, G.C.: Enhanced mobility accompanies the active deformation of a glassy amorphous polymer. *Phys. Rev. Lett.* **89**(17), 175505 (2002)
- Dusunceli, N., Colak, O.U.: Modelling effects of degree of crystallinity on mechanical behavior of semicrystalline polymers. *Int. J. Plast.* **24**(7), 1224–1242 (2008)
- Felder, S., Vu, N.A., Reese, S., et al.: Modeling the effect of temperature and degree of crystallinity on the mechanical response of Polyamide 6. *Mech. Mater.* **148**, 103476 (2020)
- Fukushima, R., Yamada, Y., Kageyama, K., et al.: Effect of heat treatment on mechanical properties of carbon-fiber-reinforced thermoplastic. *Adv. Compos. Mater.* **30**(6), 527–543 (2021)
- Galeski, A.: Strength and toughness of crystalline polymer systems. *Prog. Polym. Sci.* **28**(12), 1643–1699 (2003)
- Higuchi, Y.: Stress Transmitters at the molecular level in the deformation and fracture processes of the lamellar structure of polyethylene via coarse-grained molecular dynamics simulations. *Macromolecules* **52**, 6201–6212 (2019)
- Hoover, W.G.: Canonical dynamics: equilibrium phase-space distributions. *Phys. Rev. A* **31**(3), 1695–1697 (1985)
- Hossain, D., Tschopp, M.A., Ward, D.K., et al.: Molecular dynamics simulations of deformation mechanisms of amorphous polyethylene. *Polymer* **51**(25), 6071–6083 (2010)
- Ikeshima, D., Nishimori, F., Yonezu, A.: Deformation modeling of polyamide 6 and the effect of water content using molecular dynamics simulation. *J. Polym. Res.* **26**(6), 1–11 (2019)
- In-Chul, Y., Andzelm, J.W., Rutledge, G.C.: Mechanical and structural characterization of semicrystalline polyethylene under tensile deformation by molecular dynamics simulations. *Macromolecules* **48**(12), 4228–4239 (2015)
- In-Chul, Y., Lenhart, J.L., Rutledge, G.C., et al.: Molecular dynamics simulation of the effects of layer thickness and chain tilt on tensile deformation mechanisms of semicrystalline polyethylene. *Macromolecules* **50**(4), 1700–1712 (2017)
- Jorgensen, W.L., Maxwell, D.S., Tirado-Rives, J., Chem, J.A.: Development and testing of the OPLS all-atom force field on conformational energetics and properties of organic liquids. *Società* **118**, 11225 (1996)
- Khare, K.S., Phelan, F.R. Jr.: Integration of atomistic simulation with experiment using time-temperature superposition for a cross-linked epoxy network. *Macromol. Theory Simul.* **29**(2), 1900032 (2020)
- Kohji, T.: Molecular theory of mechanical properties of crystalline polymers. *Prog. Polym. Sci.* **18**(3), 377–435 (1993)
- Kong, Y., Hay, J.N.: The measurement of the crystallinity of polymers by DSC. *Polymer* **43**(14), 3873–3878 (2002)
- Koyanagi, J., Takase, N., Mori, K., Sakai, T.: Molecular dynamics simulation for the quantitative prediction of experimental tensile strength of a polymer material. *Composites, Part C* **2**, 100041 (2020)
- Liu, J., Cao, D., Zhang, L., et al.: Time-temperature and time-concentration superposition of nanofilled elastomers: a molecular dynamics study. *Macromolecules* **42**(7), 2831–2842 (2009)
- Mahajan, D.K., Singh, B., Basu, S.: Void nucleation and disentanglement in glassy amorphous polymers. *Phys. Rev. E, Stat. Nonlinear Soft Matter Phys.* **82**(1 Pt 1), 011803 (2010)
- Moyassari, A., Gkourmpis, T., Hedenqvist, M.S., et al.: Molecular dynamics simulations of short-chain branched bimodal polyethylene: topological characteristics and mechanical behavior. *Macromolecules* **52**(3), 807–818 (2018)
- Moyassari, A., Gkourmpis, T., Hedenqvist, M.S., et al.: Molecular dynamics simulation of linear polyethylene blends: effect of molar mass bimodality on topological characteristics and mechanical behavior. *Polymer* **161**(14), 139–150 (2019)
- Moyassari, A., Gkourmpis, T., Hedenqvist, M.S., Gedde, U.W.: Molecular dynamics simulation of linear polyethylene blends: effect of molar mass bimodality on topological characteristics and mechanical behavior. *Polymer* **161**, 139–150 (2019)
- Nitta, K.: A molecular theory of stress-strain relationship of spherulitic materials. *Comput. Theor. Polymer Sci.* **9**(1), 19–26 (1999)
- Nitta, K.-H., Nomura, H.: Stress-strain behavior of cold-drawn isotactic polypropylene subjected to various drawn histories. *Polymer* **55**, 6614–6622 (2014)
- Nosé, S.: A unified formulation of the constant temperature molecular-dynamics methods. *J. Chem. Phys.* **81**(1), 511–519 (1984)
- O'Connor, T.C., Robbins, M.O.: Chain ends and the ultimate strength of polyethylene fibers. *ACS Macro Lett.* **5**(3), 263–267 (2016)
- Pan, Y., Gao, X., Lei, J., et al.: Effect of different morphologies on the creep behavior of high-density polyethylene. *RSC Adv.* **6**(5), 3470–3479 (2016)
- Parenteau, T., Ausias, G., Grohens, Y., et al.: Structure, mechanical properties and modelling of polypropylene for different degrees of crystallinity. *Polymer* **53**(25), 5873–5884 (2012)

- Rahman, M., Parrinello, A.: Crystal structure and pair potentials: a molecular-dynamics study. *Phys. Rev. Lett.* **45**(14), 1196–1199 (1980)
- Sakai, T., Somiya, S.: Analysis of creep behavior in thermoplastics based on visco-elastic theory. *Mech. Time-Depend. Mater.* **15**(3), 293–308 (2011)
- Sakai, T., Hirai, Y., Somiya, S.: Estimating the creep behavior of glass-fiber-reinforced polyamide considering the effects of crystallinity and fiber volume fraction. *Mech. Adv. Mater. Mod. Process.* **4**(1), 1–9 (2018)
- Sakai, T., Shamsudim, N.S.B., Fukushima, R., et al.: Effect of matrix crystallinity of carbon fiber reinforced polyamide 6 on static bending properties. *Adv. Compos. Mater.* **30**(sup2):71–84 (2021)
- Shang, Y., Zhang, X., Xu, H., et al.: Microscopic study of structure/property interrelation of amorphous polymers during uniaxial deformation: a molecular dynamics approach. *Polymer* **77**, 254–265 (2015)
- Somiya, S., Yamada, K., Sakai, T.: Bending creep deformation of glass fiber reinforced polyoxymethylene. *Innovative Developments Characterizations and Applications of Composites*, 239–249 (2006)
- Tábi, T., Hajba, S., Kovács, J.G.: Effect of crystalline forms ( $\alpha'$  and  $\alpha$ ) of poly(lactic acid) on its mechanical, thermo-mechanical, heat deflection temperature and creep properties. *Eur. Polym. J.* **82**, 232–243 (2016)
- Um, H.-J., Hwang, Y.-T., Choi, K.H., et al.: Effect of crystallinity on the mechanical behavior of carbon fiber reinforced polyethylene-terephthalate (CF/PET) composites considering temperature conditions. *Compos. Sci. Technol.* **207**(3), 108745 (2021)
- Vu-Bac, N., Lahmer, T., Keitel, H., et al.: Stochastic predictions of bulk properties of amorphous polyethylene based on molecular dynamics simulations. *Mech. Mater.* **68**, 70–84 (2014)
- Yeh, I.C., Balzano, L., Harm van der Werff, R.A., et al.: Effects of finite lengths of chains on the structural and mechanical properties of polyethylene fibers. *Macromolecules* **53**(1), 18–28 (2020)

**Publisher's Note** Springer Nature remains neutral with regard to jurisdictional claims in published maps and institutional affiliations.

Springer Nature or its licensor (e.g. a society or other partner) holds exclusive rights to this article under a publishing agreement with the author(s) or other rightsholder(s); author self-archiving of the accepted manuscript version of this article is solely governed by the terms of such publishing agreement and applicable law.